DOI: 10.53469/jtpes.2023.03(09).02

Preparation and Catalytic Performance of Cu-Doped TiO_2-g-C_3N_4 Composites

Saihe Yang[1,a], Yifei Zhang[2,b]

[1]Puyang Institute of Technology, Henan University, Puyang 457004, China
[2]Saint Petersburg State University of Architecture and Civil Engineering, Saint Petersburg 190005, Russia
[a]*h2031376756@163.com*, [b]*zyf757704382@163.com*

Abstract: ***Photocatalytic methods present a viable solution for mitigating global energy deficits and environmental concerns. Therefore, it is crucial to develop effective photocatalytic systems and related materials. Among various options, semiconductor photocatalysts have gained attention due to their straightforward synthesis, economic viability, and eco-friendly nature. Key examples include the metal oxide semiconductor TiO_2 and the non-metallic counterpart, g-C_3N_4. This research focuses on creating a TiO_2/g-C_3N_4 binary heterojunction through a calcination process, subsequently incorporating copper (Cu) via photo-deposition to yield Cu/TiO_2/g-C_3N_4 ternary composite nanomaterials. Material characterization techniques such as scanning electron microscopy (SEM), X-ray diffraction (XRD), and UV-Visible spectroscopy confirmed the successful formation of these composites, exhibiting increased specific surface areas and heightened responsiveness to visible light. Additionally, the efficiency of these Cu-doped composites was evaluated through rhodamine B degradation tests, demonstrating improved visible light absorption and overall superior photocatalytic performance.***

Keywords: Photocatalytic; TiO_2-g-C_3N_4; Composite material; Deposition of light; Rhodamine B.

1. INTRODUCTION

Amid rapid technological progress and societal changes, addressing critical issues such as energy scarcity and environmental degradation has become imperative. Semiconductor photocatalysis is gaining traction as an effective strategy for mitigating these problems. Semiconducting materials like TiO_2 and graphitic carbon nitride (g-C_3N_4) are particularly attractive due to their ease of preparation, cost-effectiveness, and environmental compatibility.[1] These substances have seen diverse applications, including water treatment and atmospheric purification. Nonetheless, intrinsic limitations such as limited visible light reactivity and high rates of photogenerated carrier recombination hamper their effectiveness.[2,5]

Numerous studies have focused on TiO_2 to understand the relationship between its crystalline form and its capability to facilitate photocatalytic reactions. In contrast, g-C_3N_4, a rising player in the field of photocatalysis, displays substantial potential but requires improvements, particularly in its performance under visible light and in reducing carrier recombination rates. Combining g-C_3N_4 with other semiconductors like TiO_2 has been suggested to enhance its photocatalytic efficiency. Additionally, the integration of metal co-catalysts presents another promising approach; although gold (Au) is highly effective, its high cost makes it less feasible for broad application. As a result, alternative, cost-effective metals like copper (Cu) have garnered academic attention.[3,6-10]

This study aims to explore the benefits of incorporating Cu into a TiO_2/g-C_3N_4 composite, supported by comprehensive material characterization and performance evaluation of the resulting compound.[4]

2. EXPERIMENT

2.1 Materials

The instruments used for the experiment are listed in Table 2.1. And the chemicals used in the experiment are shown in Table 2.2.

Table 2.1 Experimental Instruments

Instrument Name	Model	Manufacturer
Box Resistance Furnace	SX2−4−10N	Beijing Zhongxing Weiye Instrument Co., Ltd.
Centrifugal Precipitator	80-2	Gongyi City Yuhua Instrument Co., Ltd.

Electric Blast Drying Oven	BGZ	Shanghai Boxun Industrial Co., Ltd.
Electronic Balance	FA2004	Shanghai Shunyu Hengping Scientific Instrument Co., Ltd.
Photochemical Reactor	BL−GHX−V	Shanghai Bilang Instrument Manufacturing Co., Ltd.
Vacuum Drying Oven	DZF-6020	Shanghai Boxun Industrial Co., Ltd.
Ultrasonic Cleaner	KQ-300DB	Kunshan Ultrasonic Instruments Co., Ltd.
Magnetic Stirrer	MS300	Shanghai Bante Instrument Co., Ltd.
Muffle Furnace	NBD-M1200	NobelTech Materials Co., Ltd.

Table 2.2 Experimental Chemicals

Chemical Name	Specification	Manufacturer
Anhydrous Ethanol	Analytical Pure	Luoyang Chemical Reagent Factory
Anatase Titanium Dioxide	Analytical Pure	Shanghai Macklin Biochemical Science & Technology Co., Ltd.
Rutile Titanium Dioxide	Analytical Pure	Shanghai Macklin Biochemical Science & Technology Co., Ltd.
Graphitic Carbon Nitride	Analytical Pure	Qingdao Bangtex Fiber Co., Ltd.
Copper Nitrate	Analytical Pure	Tianjin Sheng Ao Chemical Reagent Co., Ltd.
Rhodamine B	Analytical Pure	Guangfu Fine Chemical Research Institute

2.2 Synthesis of the Composite Material

In this study, titanium dioxide (TiO_2) serves as the primary semiconductor material and is combined with graphitic carbon nitride (g-C_3N_4) to form a heterostructure. This assembly optimizes the band gap of the catalyst, subsequently facilitating the efficient generation and movement of photogenerated electrons and holes. Copper (Cu) nanoparticles are then deposited onto the heterostructure's surface through a photo-deposition process. This modification not only enhances the composite's absorption capabilities in the visible light spectrum but also allows the Cu nanoparticles to act as electronic mediators, thereby boosting the migration of photogenerated carriers across the TiO_2-g-C_3N_4 interface. The cumulative effect of these three elements results in a significant improvement in photocatalytic activity. Figure 2.1 provides an illustration detailing the construction of this Cu-enhanced TiO_2-g-C_3N_4 composite.n.[3,6-10]

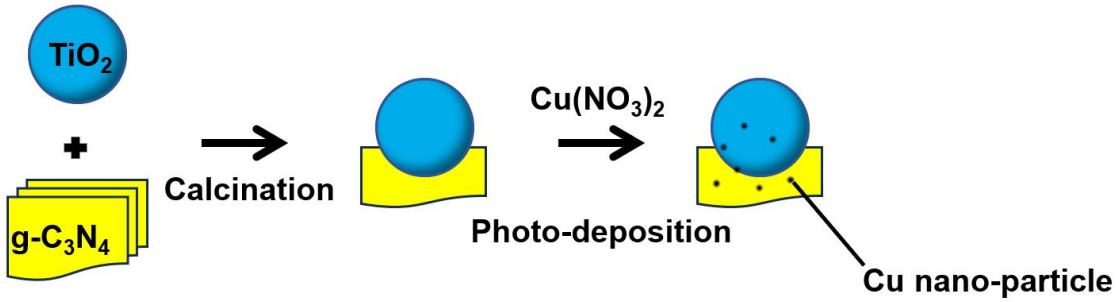

Figure 2.1: Schematic illustration of the preparation of Cu/TiO_2/g-C_3N_4

The following procedures were followed to synthesize and characterize the Cu-doped TiO_2/g-C_3N_4 composite material:

a) Initially, a homogeneous blend of 200 mg of rutile-phase titanium dioxide (TiO_2) and 800 mg of graphitic carbon nitride (g-C_3N_4), sourced from urea, was ground to form a fine powder. This powder was uniformly laid out in a crucible and heated in a muffle furnace at a rate of 5°C per minute, reaching and maintaining 500°C for three hours. After cooling to room temperature, a light-yellow substance, identified as the TiO_2/g-C_3N_4 precursor, was obtained.[12]

b) To incorporate Cu nanoparticles, a photo-deposition method was utilized. An aliquot of 200 mg of the precursor was dissolved in 50 mL of deionized water, creating a consistent dispersion. This was followed by a stepwise addition of a $Cu(NO_3)_2 \cdot 3H_2O$ solution under constant agitation. Exposing the blend to a 300W xenon lamp for one hour carried out the deposition, and a temperature-controlled glass stirrer in conjunction with a cooling water circulation system maintained ambient conditions.

c) After exposure to light, the material was subjected to a series of washes with deionized water and ethanol before being centrifuged at 8000 rpm for 10 minutes. The resulting precipitate was then dried in a vacuum oven at 60℃ for an extended period of 10 hours. The end product, labeled X-Cu/TiO_2/g-C_3N_4, was cataloged, where "X" represents the fraction of Cu nanoparticles integrated into the composite.
This approach was devised to ensure a thorough and standardized preparation and analysis of the composite material.[13]

2.3 X-ray Diffraction (XRD)

In this study, X-ray diffraction (XRD) was utilized to evaluate the atomic structure and phase composition of the synthesized materials.[14] The distinctiveness of diffraction peaks depends on the crystal's atomic composition and the spatial organization within the unit cell, yielding a unique pattern for each crystal type. A Bruker D8 Advance X-ray diffractometer, originating from Germany and fitted with a CuKα radiation source (λ=1.5406Å), was used for the analyses. Before the measurements, samples were evenly spread onto a glass slide that included an inherent groove. The apparatus operated at specific settings of 45kV for voltage and 40 mA for current. For comprehensive characterization, a 2θ scanning range between 20 and 80° was chosen. This approach allowed for a detailed examination of the crystalline structures and phase constituents of the samples.[15]

2.4 Scanning Electron Microscopy (SEM)

The Scanning Electron Microscope (SEM) stands as an instrument of precision and sophistication.[16] Its foremost advantage lies in its capacity to scrutinize a vast array of samples while inflicting minimal damage or contamination. Moreover, it offers insights into the morphology, structure, composition, and crystallinity of specimens. For this study, the selected SEM model was the Field Emission Scanning Electron Microscope (FE-SEM SU8010, Hitachi, Tokyo, Japan), which facilitated the observation of sample morphology and microstructure. Samples were mounted on a copper plate using conductive adhesive prior to assessment. An operating voltage of 10kV was employed, ensuring a detailed visualization of the material's morphology and overarching structure.

2.5 Ultraviolet-Visible Diffuse Reflectance Spectroscopy (UV-vis DRS)

Ultraviolet-visible diffuse reflectance spectroscopy (UV-vis DRS) elucidates the absorption intensity of composite materials throughout the UV-visible light spectrum.[20] From the UV-vis DRS spectra, the light absorption capacity of a material at specific wavelengths becomes evident. In this study, the Lambda 950 Ultraviolet-Visible-Near Infrared (UV-Vis-NIR) spectrophotometer was employed for the UV-vis DRS analysis of samples, with barium sulfate ($BaSO_4$) serving as the reference material.

To prepare the samples for testing, 0.02g of the material was combined with 0.2g of $BaSO_4$. This blend was meticulously ground using a mortar and pestle. The resulting mixture was then compressed onto a UV quartz plate to create a compact disc, which was subsequently analyzed using the Lambda 950 UV-Vis-NIR spectrophotometer.

2.6 Photocatalytic Test

The photocatalytic performance of the prepared samples was evaluated based on their capacity to degrade a Rhodamine B solution (concentration: 10 mg·L-1) under a 300W xenon lamp. Below is an outline of the methodology employed:[17-19]

(1) Reactor Setup: A reactor coated with aluminum foil to minimize light entry was loaded with 20 mg of the pre-prepared catalysts, either binary or ternary composites.

(2) Dye Inclusion: Subsequently, 50 mL of the Rhodamine B solution was added to the reactor.

(3) Catalyst Dispersion: Ultrasonication was employed for 10 minutes to ensure uniform distribution of the catalyst particles in the dye solution.

(4) Equilibrium Establishment: The reactor's contents were magnetically agitated for 30 minutes to reach adsorption-desorption equilibrium, after which a 4 mL sample was extracted.

(5) Irradiation Process: The aluminum foil cover was removed, and the reactor was exposed to the xenon lamp for 2 hours. During this period, continuous stirring and a recirculating water cooling system were utilized to maintain a stable temperature. Samples of 4 mL were taken at half-hour intervals for analysis.

(6) Post-Irradiation Assessment: After light exposure, the samples were centrifuged to separate catalyst residues. The resulting supernatant was analyzed using UV-Visible spectrophotometry, focusing on Rhodamine B's characteristic absorption peak at 556 nm.

Analysis of the absorption intensities allowed for the assessment of Rhodamine B degradation levels. A decrease in absorption indicated higher degradation efficiency, thus providing a measure of the photocatalytic effectiveness of the respective samples.[20]

3. EXPERIMENTAL CONCLUSIONS

3.1 X-ray Diffraction (XRD)

The X-ray diffraction analysis of 5% Cu/TiO_2/g-C_3N_4, (J)TiO_2/g-C_3N_4, and (R)TiO_2/g-C_3N_4 composites, as shown in Figure 3.1, reveals several noteworthy aspects regarding their crystalline structures. When compared to reference spectra, these materials display diffraction patterns aligning with known TiO_2/g-C_3N_4 and Cu/TiO_2/g-C_3N_4 phases. The enhanced breadth and intensity of these peaks, compared to those of pure TiO_2 and g-C_3N_4, suggest improved light absorption properties in these composites.

Specifically, diffraction peaks at 2θ values of 25.4°, 37.7°, 48.2°, 53.9°, 55.1°, 62.7°, 70.3°, and 75.1° are in agreement with the anatase phase of TiO_2, confirming its predominant role in these synthesized materials. Additionally, a characteristic peak of g-C_3N_4 manifests at a 2θ value of 27.7°, confirming successful integration with TiO_2. Contrarily, the absence of discrete Cu peaks in the Cu/TiO_2/g-C_3N_4 composite suggests minimal Cu incorporation or its thorough dispersion on the TiO_2 framework.[21]

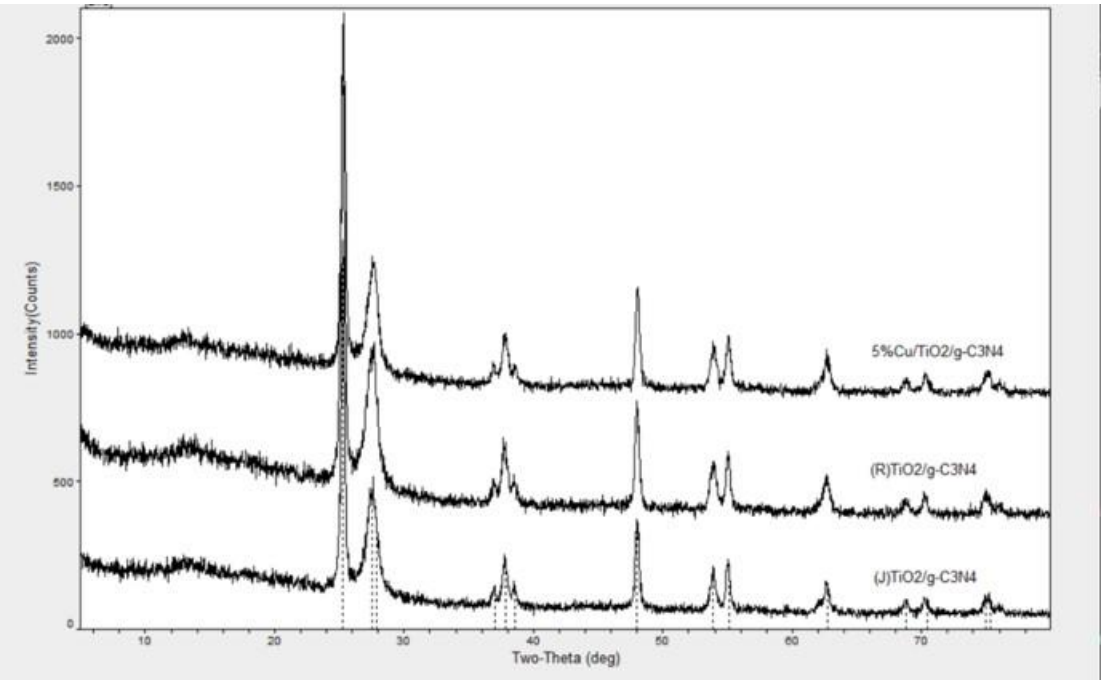

Figure 3.1 X-ray Diffraction Patterns. (J)TiO_2 represents the rutile phase of TiO_2, while (R)TiO_2 denotes the anatase phase of TiO_2

3.2 Scanning Electron Microscopy (SEM)

Figure 3.2 showcases the scanning electron microscopy (SEM) depiction of the anatase phase TiO_2/g-C_3N_4. In this representation, TiO_2 manifests as spherical entities, stemming from the agglomeration of minute TiO_2 nanoparticles to create consistently structured spheroidal particles. Observably, from Figure 3.2, deposits can be

identified on these spheroidal particle surfaces, alluding to the establishment of a TiO_2/g-C_3N_4 binary heterojunction catalyst. The pronounced surface roughness augments the catalyst's specific surface area, thus bolstering its catalytic efficiency.

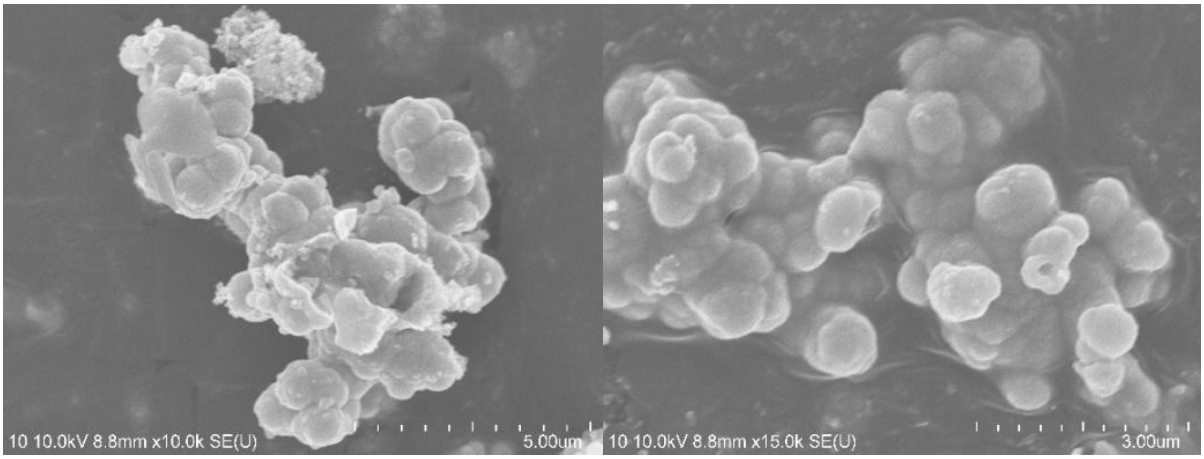

Figure 3.2 Scanning Electron Microscopy (SEM) image of the anatase phase TiO_2/g-C_3N_4

Figure 3.3 displays the Scanning Electron Microscopy (SEM) representation of the Cu-modified TiO_2-g-C_3N_4 nanocomposite. This depiction reveals the dispersion and morphological characteristics of the Cu/TiO_2/g-C_3N_4 composite material. As elucidated in Figure 3.3, the composite showcases an enhanced dispersion, augmented specific surface area, and an abundance of reactive active sites. Nonetheless, a consistent morphology remains elusive. Potential explanations for this irregularity encompass: (1) the pronounced dispersion of Cu nanoparticles on the TiO_2/g-C_3N_4 substrate; (2) alterations in the TiO_2/g-C_3N_4 heterojunction structure consequent to Cu doping; and (3) the amalgamation of TiO_2/g-C_3N_4 composites subjected to varied calcination periods.

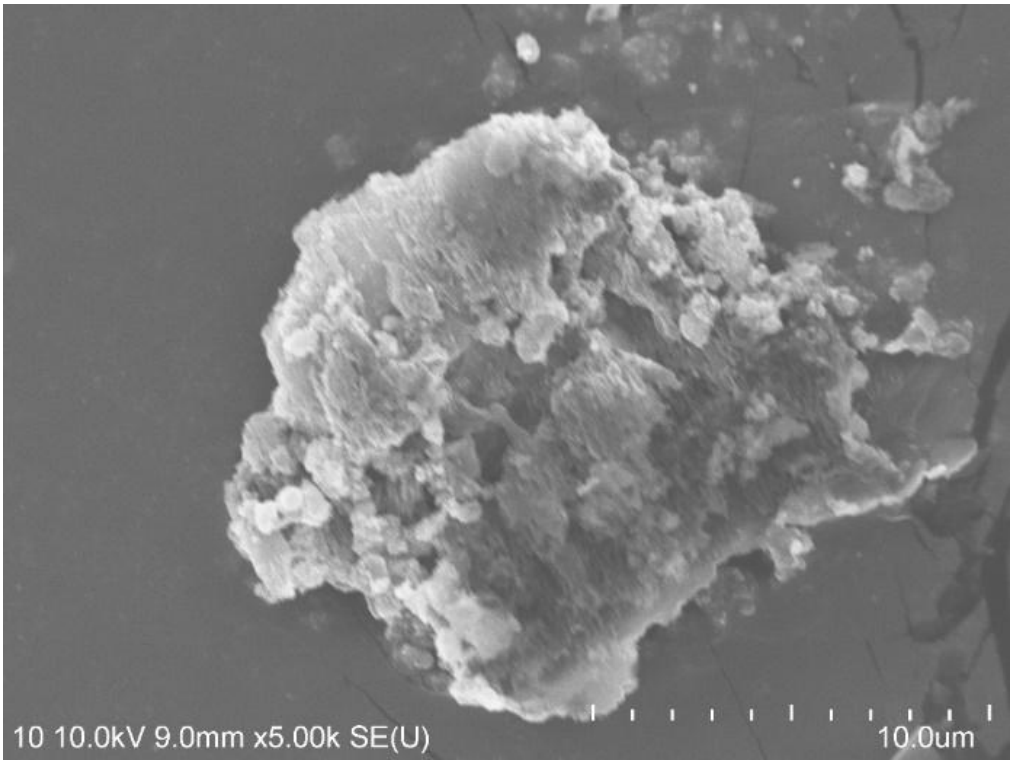

Figure 3.3 SEM image of the 5% Cu/TiO_2/g-C_3N_4 composite material

3.3 Ultraviolet-Visible Diffuse Reflectance Spectroscopy (UV-vis)

The photocatalytic attributes of the composite nanomaterials were assessed using UV-visible diffuse reflectance spectroscopy. Spectra for the rutile phase TiO2/g-C3N4 composite, the anatase phase TiO_2/g-C_3N_4 composite, and the 5% Cu-modified TiO_2/g-C_3N_4 composite are depicted in Figure 3.4, where the vertical axis delineates light absorption intensity and the horizontal axis indicates wavelength.

Figure 3.4 reveals that the binary composites, absent of Cu doping, manifest pronounced absorption intensities for wavelengths below 330 nm. Intriguingly, the absorption intensity for the anatase phase TiO_2/g-C_3N_4 composite marginally surpasses that of its rutile counterpart, leading to its selection for Cu doping in subsequent investigations. Post metallic Cu deposition, the absorption spectrum widened, notably displaying appreciable absorption intensities for wavelengths exceeding 400 nm in the visible light domain. Such observations underscore that the Cu-modified TiO_2/g-C_3N_4 composite nanomaterial proffers augmented light absorption capabilities.

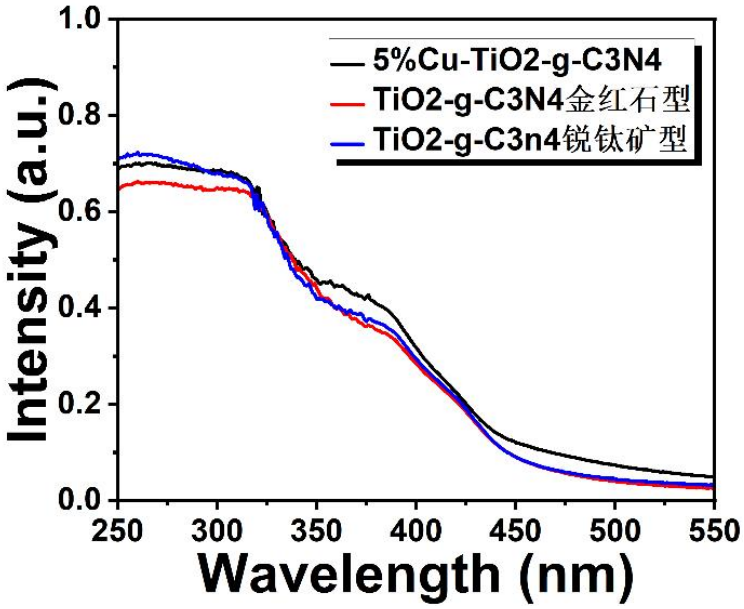

Figure 3.4 UV-Visible Diffuse Reflectance Spectra of the prepared binary TiO_2/g-C_3N_4 composite and the ternary Cu-modified TiO_2/g-C_3N_4 nanocomposite

3.4 Photocatalytic Performance Study

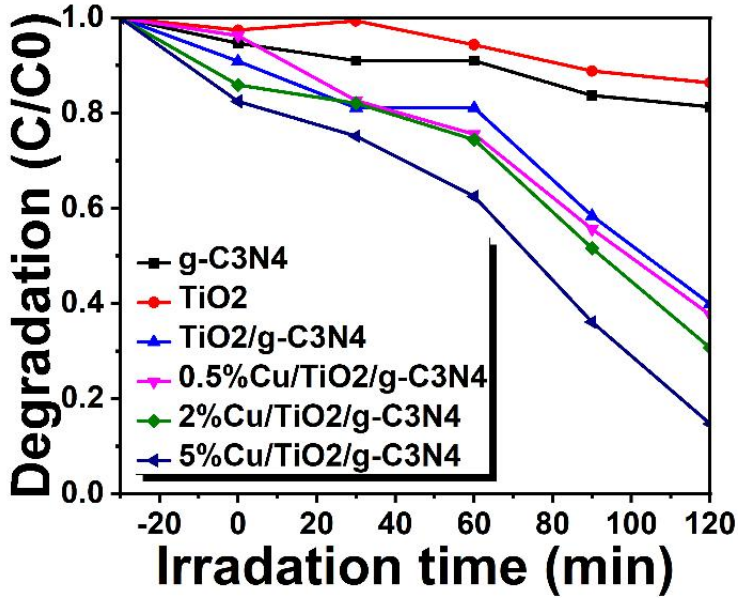

Figure 3.5 Degradation profile of Rhodamine B

The photocatalytic performance of various composites was quantified through Rhodamine B degradation under a xenon lamp, as depicted in Figure 3.5. The vertical axis represents the rate of degradation, while the horizontal axis indicates illumination time. When utilizing g-C_3N_4, TiO_2, TiO_2/g-C_3N_4, and Cu/TiO_2/g-C_3N_4, a steady decline in Rhodamine B concentration was recorded. The solo activities of TiO_2 and g-C_3N_4 yielded suboptimal results, with less than 20% degradation efficiency at the 120-minute measurement point. Conversely, the TiO_2/g-C_3N_4 binary composite demonstrated significant improvement, achieving nearly 60% degradation efficiency. The addition of Cu to the composite further elevated its ability to degrade Rhodamine B, highlighting the enhanced photocatalytic potential of this ternary system relative to its binary and individual material counterparts.[23]

Further examination demonstrated a positive link between the metallic Cu content and the composite's photocatalytic efficiency within the observed parameters. Figure 3.6 reveals that a ternary system with 5% Cu achieved an 80% Rhodamine B degradation rate after 120 minutes of light exposure. This performance boost is potentially attributed to the surface plasmon resonance (SPR) effect of the Cu nanoparticles. In addition, Cu's conductive nature acts as an electron transport medium, facilitating electron movement between TiO_2 and g-C_3N_4, thus enhancing charge separation and catalytic action.

In the study, various Cu concentrations—0.5%, 2%, and 5%—were introduced into the TiO_2/g-C_3N_4 heterojunction via photo-deposition. Optimal photocatalytic behavior was reached at 5% Cu concentration, as indicated in Figure 3.6. Nevertheless, an excess of Cu can cause saturation, reducing efficiency. Under such circumstances, Cu entities may serve as charge recombination sites, hindering the efficient separation of photogenerated carriers and compromising the catalyst's performance. Therefore, while Cu doping improves photocatalytic activity, there is an optimum concentration beyond which performance may diminish.

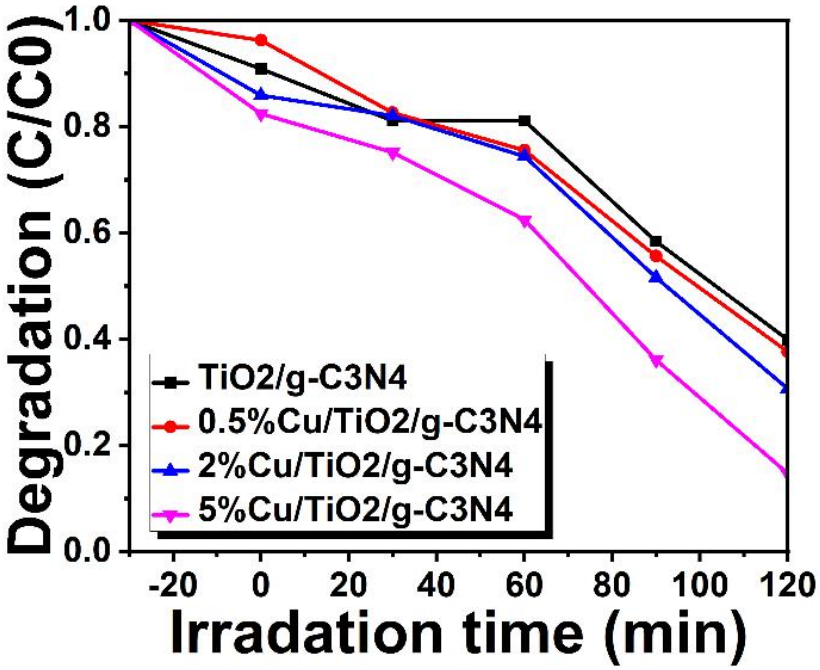

Figure 3.6 Comparison of photocatalytic efficiencies of Cu/TiO_2/g-C_3N_4 composite materials prepared with varying concentrations of doped metallic Cu

4. CONCLUSION

In this investigation, TiO_2, g-C_3N_4, and $Cu(NO_3)_2 \cdot 3H_2O$ served as the initial reactants. Anatase and rutile forms of TiO_2/g-C_3N_4 composites were first prepared using calcination. Spectroscopic analysis with UV-visible diffuse reflectance indicated that the photocatalytic performance of the rutile composite modestly exceeded that of its anatase equivalent. We then proceeded to synthesize Cu-doped TiO_2-g-C_3N_4 using a photo-deposition technique with the rutile form.

To scrutinize the microstructure and dispersion of Cu-doped TiO_2-g-C_3N_4, scanning electron microscopy (SEM) was used. The findings revealed better nanoparticle dispersion, a greater specific surface area, and more reactive

sites. X-ray diffraction (XRD) results corroborated these structural details and indicated improved absorption intensity. The rutile-based composite outperformed its anatase equivalent in terms of light absorption. After Cu doping, the material displayed enhanced absorption across a broader spectrum, especially for wavelengths beyond 400 nm.

Comparative tests elucidated that the Cu-doped ternary system demonstrated superior photocatalytic capabilities relative to the individual components or their binary mix. Exploration with varying Cu levels indicated that an optimal concentration range exists, within which photocatalytic efficiency positively correlated with the amount of Cu incorporated.

REFERENCES

[1] Bo Zhou. Preparation and performance study of titanium dioxide/graphitic phase carbon nitride-based composite photocatalysts [D]. Changchun, Jilin: Jilin University, 2019.

[2] Zili Xu. Preparation of molecularly modified carbon nitride/titanium dioxide composites and visible photocatalytic performance study [D]. Wuhan, Hubei: Huazhong University of Science and Technology, 2018.

[3] Feng Zhang. oluene liquid-phase oxidation catalysed by copper-modified graphitic carbon nitride materials [J]. Guangdong Chemical, 2017, 44(12): 124, 127-128.

[4] Guang Ping. Preparation of graphene-loaded TiO2-NX/Cu2O composite photocatalysts [J]. Shanxi Chemical Industry, 2019(6): 662-666.

[5] Yumin Cui. Preparation of g-C3N4/TiO2 composite photocatalyst and its performance study [J]. Applied Chemistry，2014(8): 1047-1396.

[6] Guoli Fang, Mengyue Li, Hongfang Shen, Shaolin Yang, Jahanzaib Israr. Enhanced photocatalytic characteristics and low selectivity of a novel Z-scheme TiO2/g ? C3N4/Bi2WO6 heterojunction under visible light[J]. Materials Science in Semiconductor Processing, 2021: 1-8.

[7] Peng Deng. Effect of Au, Cu and Cu oxide modifications on the photocatalytic activity of TiO2 [D]. Chengdu, Sichuan: University of Electronic Science and Technology of China,2019.

[8] Dong Yan, Xin Wu, Jiayun Pei, Chaochao Wu, Xiumei Wang, Haiyan Zhao. Construction of g-C3N4/TiO2/Ag composites with enhanced visible-light photocatalytic activity and antibacterial properties[J]. Ceramics International, 2020(46): 696-702.

[9] Jin Zhang. Photoelectrocatalytic degradation of ofloxacin in water by copper ion doped titanium dioxide nanotubes [D]. Dalian Maritime University, 2020.

[10] Lili Zheng, Xinyan Xiao, Yang Li, Weiping Zhang. Enhanced photocatalytic activity of TiO2 nanoparticles using WS2/g-C3N4 hybrid as co-catalyst[J]. Science Direct, 2017(27): 1117-1126.

[11] Zhibin Liu. Study on the degradation properties of cefoperazone by copper-doped titanium dioxide [J]. Journal of Harbin University of Commerce (Natural Science Edition), 2019, 35(6): 662-666.

[12] Iran Ali, Seongjun Park, Jong-Oh Kim. Modeling the photocatalytic reactions of g-C3N4-TiO2 nanocomposites in a recirculating semi-batch reactor[J]. Journal of Allors and Compounds, 2020(821): 1-10.

[13] Jvfeng Lou. Synthesis of metal-doped graphitic phase carbon nitride nanomaterials and their application in degrading pollutants [D]. Jinhua, Zhejiang: Zhejiang Normal University, 2019.

[14] Huijun Liang. Selective photocatalytic activity and mechanism of Ag/TiO2-based composites [D]. Xinxiang prefecture level city in Henan: Henan Normal University, 2018.

[15] Hang Li. Preparation of gold-doped titanium dioxide nanoparticles and study of their surface enhancement effect [D]. Mianyang, Sichuan: Chinese Academy of Engineering Physics (CAEP), 2019.

[16] Low J, Yu J, Jaroniec M, et al. Heterojunction Photocatalysts[J]. Advanced Material, 2017, 29(20): 1061694.

[17] Rudan Hu. Preparation and electrochemical properties of cobalt-doped manganese oxide aqueous zinc ion battery cathode materials [J]. Mechanical engineering materials, 2021(01).

[18] Dayu Li. Progress of photocatalytic properties of different kinds of metal-doped modified TiO2 materials [J]. Materials Herald, 2019(23).

[19] Jianjun Liu. First-principles study of heterostructure, doping and nanotube structure of g-C3N4 photocatalytic materials [D]. Wuhan, Hubei: Wuhan Institute of Technology, 2017.

[20] Jiaxin Ni. Preparation of g-C3N4/TiO2 photocatalysts and study of visible light degradation of TCH in water [D]. Harbin, Heilongjiang: Harbin Institute of Technology, 2019.

[21] Shengnan Fan. Preparation and characterisation of three cellulose-based activated carbon fibres [J]. Journal of Chemical Engineering in Higher Education, 2021(02).

[22] Zhen Qin. Zinc-doped g-C3N4/BiVO4 as a Z-scheme photocatalyst system for water splitting under visible light[J]. Chinese Journal of Catalysis, 2018(39): 472–478.

[23] Naixu Li. MgO and Au nanoparticle Co-modified g-C3N4 photocatalysts for enhanced photoreduction of CO2 with H2O[J]. Chinese Journal of Catalysis, 2021(42): 781–794.